Biomedical Signal Processing and Control 101 (2025) 107238

Contents lists available at ScienceDirect

Biomedical Signal Processing and Control

journal homepage: www.elsevier.com/locate/bspc

Detection of interictal epileptiform discharges using transformer based deep neural network for patients with self-limited epilepsy with centrotemporal spikes

Pei Feng Tong [a,1], Bosi Dong [b,1], Xiangdong Zeng [c], Lei Chen [b,d,*], Song Xi Chen [e,**]

[a] Guanghua School of Management, Peking University, Beijing 100871, China
[b] Department of Neurology, West China Hospital, Sichuan University, Chengdu 610041, China
[c] Department of Pediatric Neurology, Chengdu Women's and Children's Central Hospital, School of Medicine, University of Electronic Science and Technology of China, Chengdu 611731, China
[d] Pazhou Lab, Guangzhou 510330, China
[e] Department of Statistics and Data Science, Tsinghua University, Beijing 100084, China

ARTICLE INFO

Keywords:
Automated detection
Deep learning
Independent component analysis
SeLECTS
Spike detection

ABSTRACT

Objective: Scalp-visible interictal epileptiform discharges (IEDs) are known to be crucial for the diagnosis of self-limited epilepsy with centrotemporal spikes (SeLECTS). However, labeling and mapping these discharges over electroencephalography (EEG) recordings are repetitive and time-consuming, requiring much tedious and careful efforts. Fully automated IEDs detection algorithm with high accuracy and generalization ability is much desired.
Methods: We designed an efficient data preprocessing-feature extraction-classification workflow, which is composed by the independent component analysis, clinical knowledge-based waveform dictionary and transformer based deep neural network classifier, to identify the timing and recording electrode associated with each individual IEDs and the dipole patterns.
Results: A total of 44,908 IEDs labeled within video EEG recordings were collected from 25 SeLECTS patients. The proposed procedure achieved an averaged accuracy of 99.8% and sensitivity of 97.8% in the test dataset consisting of 8 patients, with the false alarm rate been 1.8 per hour for nonepileptic EEG recordings. All the eight SeLECTS patients in the test set have been detected dipole pattern and five of them is found to have IEDs frequencies 10 times higher in sleep stage compared with the awake period. The generalization ability of the procedure is further confirmed through a cross-dataset evaluation in the publicly available TUEV dataset.
Conclusions: The proposed fully automated IEDs detection procedure shows high accuracy and good generalization ability.
Significance: The proposed procedure can significantly lower the work burden of neurologists and provide a quantitative tool for IEDs analysis in further epilepsy research.

1. Introduction

Self-limited epilepsy with centrotemporal spikes (SeLECTS) is one of the most common forms of epilepsy reported in the children [1]. SeLECTS accounts for up to 23 % of childhood epilepsy, which is often associated with developmental disorders [2]. The typical age of SeLECTS onset is between 3 and 12 years, and the remission typically occurs by the early teenage years, with genetic predisposition and male predominance [3]. SeLECTS is characterized by normal background with high-amplitude centrotemporal spikes or sharp waves on the

Abbreviations: ACC, accuracy; CWCCH, Chengdu Women's and Children's Central Hospital; EEG, electroencephalography; FAR, false alarm rate; FN, false negative; FP, false positive; IEDs, interictal epileptiform discharges; MLP, multilayer perceptron; PPSI, preceding positive spike index; SeLECTS, self-limited epilepsy with centrotemporal spikes; SENS, sensitivity; SPEC, specificity; TP, true positive; VEEG, video-EEG; WCH, West China Hospital.

* Corresponding author at: Department of Neurology, West China Hospital, Sichuan University, Chengdu 610041, China
** Corresponding author at: Department of Statistics and Data Science, Tsinghua University, Beijing 100084, China
E-mail addresses: leilei_25@126.com (L. Chen), csx@gsm.pku.edu.cn (S.X. Chen).
[1] Pei Feng Tong and Bosi Dong contribute equally to this work.

https://doi.org/10.1016/j.bspc.2024.107238
Received 5 November 2023; Received in revised form 25 July 2024; Accepted 17 November 2024
Available online 25 November 2024

electroencephalogram (EEG), which are more activated in drowsiness and sleep periods [4]. Clinical seizure onsets are rare in SeLECTS and are difficult to capture, even with long-term video-EEG (VEEG) monitoring [5]. It should be considered in the differential diagnosis of focal seizures due to structural brain abnormality. According to the guidelines on childhood onset epilepsy syndromes [6], accurate detection and mapping of interictal epileptiform discharges (IEDs) are critical for the diagnosis of SeLECTS. Here, we define the mapping of IEDs as the localization of IEDs on EEG electrodes, distinct from the localization of the actual discharge position intracranially. Up till now, the interpretation of IEDs in long-term EEG relies primarily on experienced neurologists, which entails much tedious manual effort [7].

In recent years, automated detection approaches have been proposed to alleviate labor force in detecting scalp-visible IEDs [8,9]; see [10–12] for recent reviews. The existed IEDs detection studies can be classified into three groups: (1) template matching; (2) feature extraction and classification and (3) the end-to-end neural network. The template matching approach was introduced by Stevens, et al. [13] for IEDs detection, which matched EEG signals with pre-defined spike and background templates to emulate the visual inspections conducted by neurologists [14]. Apart from direct template matching, the feature extraction approach utilizes spatial–temporal or time–frequency information to capture potential invisible features. Some of the studies included the optimal template matching and morphological feature selection [15], spatial–temporal-frequency multidomain information [16], and the empirical mode decomposition [17]. The end-to-end neural networks combined feature extraction with classifier, employing the convolution neural networks (CNN) [8,9,18], the long short-term memory networks [19] and the graph neural networks [20] as the network architecture. Recently, the combination of CNN and self-attention structures has been shown to achieve better model performance with a more compact model architecture [21]. Compared with the previous two groups, the end-to-end neural networks are fully data driven but lack clinical interpretability.

The generalization ability of an automatic procedure is important for its clinical applicability as it mimics the clinic situation of neurologists every day. Since the IEDs morphology varies across patients [22], a robust procedure should demonstrate better performance on new and unseen patients who are not included in the training process. Up to now, only a few studies have evaluated their performance across out-sample patients [19,23,24]. It is also fairer to evaluate the performance at the individual patient level rather than relying solely on a proportion of the pooled data segments [25].

Temporal resolution is a crucial factor in data preprocessing, particularly in the context of classifying time series data. To enable effective classification, temporal data segmentation is necessary, where epochs are annotated and classified at the epoch level. The duration of IEDs typically ranges from 200 ms to 20 ms, which means that any epoch length greater than 200 ms may fail to distinguish individual IEDs, especially considering that multiple IEDs can occur within a single second. Previous studies have used various epoch lengths, ranging from 30 s [19] to 300 ms [26]. For example, [8,9,21] chose non-overlapping 1 s segments as input, where their algorithms determined whether each segment contained IEDs. If a segment contained multiple IEDs or high amplitude artifacts, deriving accurate measurements such as width, peak location, or amplitude of an individual IED from the detected IED segment could be challenging. Nonetheless, finer time resolution is required for accurately characterizing the statistical properties of individual IEDs.

To circumvent the shortcomings described above, we have designed an accurate and fully automatic procedure for detecting and mapping IEDs, which may help in the diagnosis of SeLECTS. The proposed procedure extracted spatial–temporal features by a clinical knowledge based waveform dictionary, which has demonstrated effectiveness in seizure detection [27]. A Transformer [28] based network structure is applied as the classifier for dealing with temporal dependencies. To achieve a finer temporal resolution, we employ a sliding window approach with a width of 760 ms and a step size of 100 ms. This choice ensures that the wider window encompassed the entire spike event and subsequent slow-wave component, while the narrower step size enables a more detailed description of each individual IED. Extensive empirical evaluations are applied on both a private dataset and a public available IEDs dataset [29], and the cross-patient and cross-dataset evaluations have been conducted to demonstrate a superior model generalization ability.

2. Materials and methods

2.1. Private dataset

The private data for this study was obtained from the Epilepsy Monitoring Units at West China Hospital (WCH) of Sichuan University and Chengdu Women's and Children's Central Hospital (CWCCH) over the period from April 2022 to June 2023. Patients who were diagnosed with SeLECTS and had IEDs in VEEG recordings were included. There were 17 males and 8 females with an average age of 9.04 ± 2.09 years in SeLECTS group. To challenge the algorithm, we also included 26 patients (15 males and 11 females; mean age 10.48 ± 4.31 years) who had normal EEG recordings, yet featured nonepileptiform sharp transients such as spiky fluctuation of the background (with patients number $n = 1$), artifacts ($n = 6$), ciganek waves ($n = 2$), small sharp spikes ($n = 3$), 6 or 14 Hz ($n = 7$), rhythmic midtemporal theta bursts of drowsiness ($n = 5$), and immature spike and waves ($n = 2$). Among all the EEG recordings, 42 recordings including 18 SeLECTS and 24 nonepileptic VEEG recordings were obtained from WCH, with the remaining 9 recordings comprising 7 SeLECTS and 2 nonepileptic VEEG recordings from CWCCH. The IEDs, their associated dipole pattern, and states of wakefulness or sleep were independently labeled by three epileptologists (BSD, LYH and QLH), each blind to the others' labeling decisions. Annotation consensus was reached by a majority vote, requiring at least two epileptologists for the confirmation of an IED event. Detailed descriptive statistics for the dataset are available in Table S1 of the supplementary materials.

NIHON KOHDEN video-EEG monitoring system was used to record multi-channel EEG with the sampling frequency being 1000 Hz (WCH)

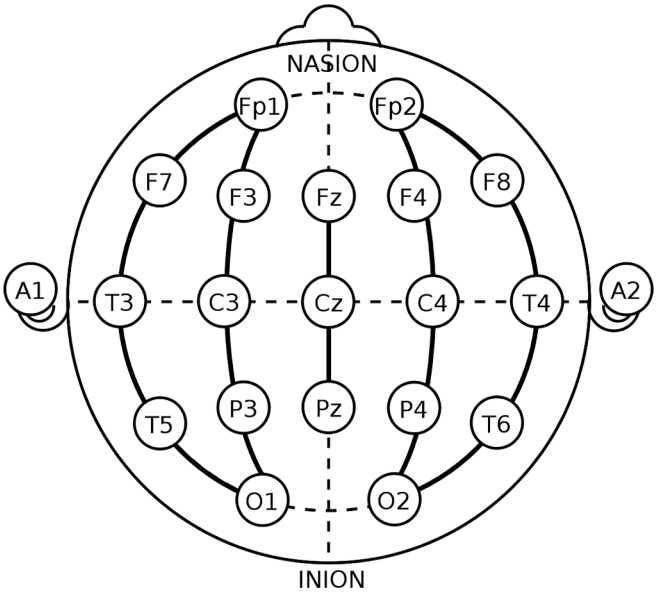

Fig. 1. Illustration of the 21 channel 10–20 system. For average reference montage, signals in each channel are subtracted by the mean of all 19 channels excluding A1 and A2. For bipolar montage, signals are referenced by longitudinal pairs, defined by the unbroken lines.

or 500 Hz (CWCCH). As shown in Fig. 1., 21 electrodes were placed in scalp following the 10–20 international standard lead system. Two types of montages, the bipolar montage (Fp1-F7、F7-T3、T3-T5、T5-O1、Fp2-F8、F8-T4、T4-T6、T6-O2、Fp1-F3、F3-C3、C3-P3、P3-O1、Fp2-F4、F4-C4、C4-P4、P4-O2、Fz-Cz、Cz-Pz) and the average reference montage, are considered for arranging the EEG channels. Long term VEEG data were randomly segmented to ensure a minimum duration of 1 h within each patient. The total duration of the included recordings was 106 h 41 min 20 s.

This study was approved by the Ethics Committee of WCH (2022169) and the Ethics Committee of CWCCH (2023109).

2.2. Public dataset

The Temple University Hospital EEG Events Corpus (TUEV) [29] is the only public scalp IEDs dataset [12], recorded using the 10–20 system with a sampling frequency of 250 Hz. This dataset was annotated with 1 s EEG segments, which can be classified to one of six categories: (1) spike and sharp wave (SPSW), (2) generalized periodic epileptiform discharges (GPED), (3) periodic lateralized epileptiform discharges (PLED), (4) eye movement (EYEM), (5) artifact (ARTF) and (6) background (BCKG). Since the temporal resolution of the labels were lower than our training requirements, the entire TUEV dataset was designated as a test data set to assess the cross-dataset generalization ability of our model.

2.3. Data preprocessing

To keep a consistent sampling frequency, all the EEG recordings were resampled at 500 Hz. Then, we passed all the EEG recordings into a Butterworth 4-th order band pass filter with the cutoff frequencies being 1 Hz and 70 Hz, respectively. A 50 Hz notch filter was also applied. Electrooculography (EOG) and electromyography (EMG) artifacts were removed by an automatic algorithm using the independent component analysis (ICA). Specifically, suppose that the total duration of observed EEG is T, let $\boldsymbol{x}_{EEG}(t) \in \mathbb{R}^{17}$, $t = 1, \cdots, T$ be the multi-channel EEG observation at time t without channels A1, A2, Fp1 and Fp2, $\boldsymbol{x}_{EOG}(t) \in \mathbb{R}^2$ be the EEG measured in prefrontal electrodes Fp1 and Fp2, $\boldsymbol{x}_{EMG}(t) \in \mathbb{R}^p$ be additional p-dimensional EMG observations. The ICA tries to solve the following linear time series model,

$$\boldsymbol{x}(t) = \boldsymbol{A}\boldsymbol{s}(t) = \boldsymbol{A}_{EEG}\boldsymbol{s}_{EEG}(t) + \boldsymbol{A}_{EOG}\boldsymbol{s}_{EOG}(t) + \boldsymbol{A}_{EMG}\boldsymbol{s}_{EMG}(t), \tag{1}$$

where $\boldsymbol{x}(t) = \left[\boldsymbol{x}_{EEG}^T(t), \boldsymbol{x}_{EOG}^T(t), \boldsymbol{x}_{EMG}^T(t)\right]^{\mathrm{T}} \in \mathbb{R}^{19+p}$ is the combined signal, $\boldsymbol{s}(t) = \left[\boldsymbol{s}_{EEG}^T(t), \boldsymbol{s}_{EOG}^T(t), \boldsymbol{s}_{EMG}^T(t)\right]^{\mathrm{T}} \in \mathbb{R}^{19+p}$ is the independent components (ICs), and $\boldsymbol{A} = [\boldsymbol{A}_{EEG}, \boldsymbol{A}_{EOG}, \boldsymbol{A}_{EMG}]$ is a squared mixing matrix. The FastICA algorithm [30] is used to estimate $\widehat{\boldsymbol{A}}$ and $\widehat{\boldsymbol{s}}(t)$, which assumes all the elements in $\boldsymbol{s}(t)$ are independent.

Intuitively, (1) tries to decompose the raw observation $\boldsymbol{x}(t)$ into three parts, and the artifact removal procedure aims to reconstruct the pure EEG part $\boldsymbol{x}^*(t) = \widehat{\boldsymbol{A}}_{EEG}\widehat{\boldsymbol{s}}_{EEG}(t)$ from the EOG/EMG contaminated observations. Given the estimated $\widehat{\boldsymbol{s}}(t)$, we can obtain $\widehat{\boldsymbol{s}}_{EOG}(t)$ ($\widehat{\boldsymbol{s}}_{EMG}(t)$) by choosing the top two (top p) ICs that have the maximum Spearman's correlation coefficients $\widehat{\rho}_{ij}$ between the i-th IC $\widehat{\boldsymbol{s}}_i(t)$ and the j-th EOG (EMG) signal $\boldsymbol{x}_{EOG,j}^T(t)$($\boldsymbol{x}_{EMG,j}^T(t)$). After excluding the 2 + p EOG/EMG ICs, the remaining 17 ICs can be chosen as the $\widehat{\boldsymbol{s}}_{EEG}(t)$.

The continuous EEG recordings were split into 0.76 s length moving windows with a step size of 0.1 s, such that two adjacent moving windows had a 0.66 s overlap. Only the initial 0.1 s of moving window determined whether it belonged to an IED or not. For model evaluation and validation, the complete dataset was divided into training set (70 %) and test set (30 %) at the patient level. Specifically, we employed the unblinded training set (26878 labeled IEDs from 17 patients and non-epileptic VEEG from 18 controls) to train the procedure for identifying IEDs and associated dipole pattern for the diagnosis of SeLECTS. The remaining private dataset (8 SeLECTSs and 8 controls) and the TUEV dataset were used as the test set to verify the generalization ability of the proposed method.

2.4. Waveform dictionary

Waveform feature series were extracted by matching the preprocessed EEG signals with a predefined waveform dictionary. To learn from the clinical knowledge on the epileptic waveforms and attain representative seizure waveform signals, we considered four basis functions $\left\{\phi_j(t)\right\}_{j=1}^4$, whose forms are given in Table 1. The inner products between the basis functions and the filtered.

EEG signals are calculated. The basis functions indicated important epileptiform discharges, which we deliberately chose the frequency range with clinical importance. Among them, the "slow component" ($j = 1$) was used to represent the "slow pattern", and the "spike/sharp component" ($j = 2$) for spike ($40 \sim 70$ms) and sharp ($70 \sim 200$ms) patterns, respectively. The "sharp/spike" ($j = 3$) was a combination of the first two components. The "Haar wave" ($j = 4$) acted to alleviate overfitting instead of being a targeted waveform. The basis functions were all compactly supported.

By utilizing these basis functions, a location-scale waveform dictionary was constructed in the form of

$$\Phi_j(t, k, \lambda) = \sqrt{\lambda}\sigma_j\left(\phi_j(t\lambda - k) - \mu_j\right), j = 1, \cdots, 4, \tag{2}$$

where k was a location shift parameter and λ is the target frequency attached within a basis $\phi_j(\cdot)$, μ_j and σ_j are the location and scale parameters in the outer layer. The waveform dictionary $\left\{\Phi_j(t, k, \lambda)\right\}_{j=1}^4$ satisfied $\sum_t \Phi_j(t) = 0$ and energy $\sum_t \Phi_j(t)^2 = 1$, echoing the admissibility conditions on the wavelet bases [31]. The selected waveforms ϕ_3 in Table 1 could be the key signatures in IEDs, especially for the slow-wave component after the sharp/spike, which is of great importance in detecting candidate IEDs clinically [32] but was often ignored by existing IEDs detection methods. The candidate frequency range of λ is provided in Table 1.

2.5. Transformer classifier

The raw EEG series, and the feature series extracted by matching with the waveform dictionary, were fed into a transformer based neural network [28] for the final classification task. As shown in Fig. 2, the designed neural network only contains encoder layers thus can focus on the classification task. The input feature series began with a multilayer perceptron (MLP) to mimic the embedding layer associated with the discontinuous language sequence, and a position embedding block then assigned the positional information to the feature series. The multi-head attention mechanism captured the relationship of the time dependence, and automatically put larger weights to the important periods. Finally, we aggregated the hidden states of the encoder layers by averaging over time with a pooling layer, followed by another MLP to obtain the final results.

2.6. Determine the dipole patterns

The existence of dipole patterns was verified once we found an IED in the Rolandic region. We propose a preceding positive spike index (PPSI) as a measure of the positive discharges in the frontal region. To be specific, the PPSI was calculated on channels F3 and F4 when IED in the Rolandic area was detected. We defined t_s and t_e to be the start and end time of a detected Rolandic IED, respectively. We then first calculated the inner product of the "sharp/spike wave" basis function (equation (2)) as

$$y_{i,\lambda}(k) = \sum_{t=-\infty}^{\infty} \Phi_2(t, k, \lambda)x_i(t), t_s \le k \le t_e, i = \mathrm{F3}, \mathrm{F4}, \lambda \in \{5, \cdots, 24\},$$

Table 1
The designed seizure waveform dictionary with the slow (ϕ_1) and the sharp/spike components (ϕ_2) as basic units. Their combination, sharp/spike wave (ϕ_3) was also considered since it had a direct association towards the seizure onset. Parameters μ_j and σ_j are chosen such that $\int \Phi dt = 0$ and $\int \Phi^2 dt = 1$, while f represent the sampling frequency, and $f = 500$ Hz for the EEG recordings.

location-scale family	waveform	Core formula $\phi_j(t)$	frequency (Hz)λ_j
$\Phi_1(t,k,\lambda_1) = \sqrt{\lambda_1}\sigma_1(\phi_1(t\lambda_1 - k) - \mu_1)$		$\phi_1(t) = \sin(\pi t/f), t \in [0,f)$	$\lambda_1 \in \{2,3,4,6,8\}$
$\Phi_2(t,k,\lambda_2) = \sqrt{\lambda_2}\sigma_2(\phi_2(t\lambda_2 - k) - \mu_2)$		$\phi_2(t) = \begin{cases} 5t/(2f), t \in [0,0.4f) \\ -5t/(3f) + 5/3, t \in [0.4f,f) \end{cases}$	$\lambda_2 \in \{5,6,\cdots,24\}$
$\Phi_3(t,k,\lambda_3^1,\lambda_3^2) = \sigma_3^{1,2}\left(\phi_3(t,k,\lambda_3^1,\lambda_3^2) - \mu_3^{1,2}\right)$		$\phi_3(t,k,\lambda_3^1,\lambda_3^2) = \phi_1\left((t - f/\lambda_3^2)\lambda_3^1 - k\right) + \phi_2(t\lambda_3^2 - k)$	$\lambda_3^1 \in \{2,3,4,6,8\}\lambda_3^2 \in \{5,7,10,15,20,25\}$
$\Phi_4(t,k,\lambda_1) = \sqrt{\lambda_4}\sigma_4(\phi_4(t\lambda_4 - k) - \mu_4)$		$\phi_4(t) = \begin{cases} 1, t \in [0,0.5f) \\ -1, t \in [0.5f,f) \end{cases}$	$\lambda_4 \in \{2,4,8,16,32,64,128\}$

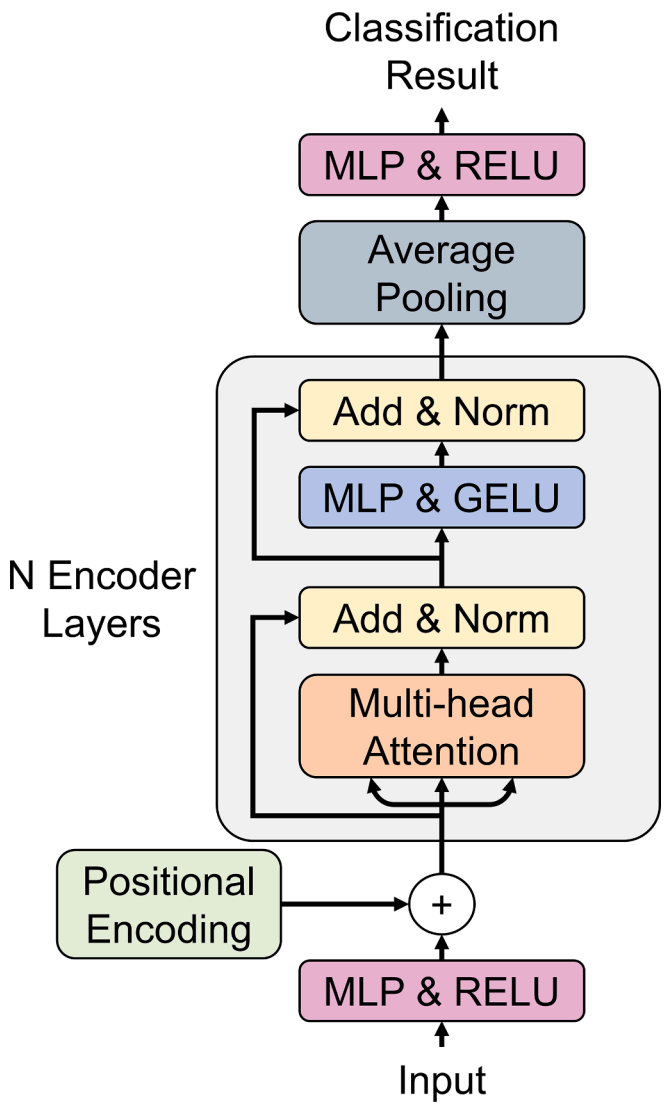

Fig. 2. Transformer structure for time series classification using only the encoder layers.

where $x_i(t)$ is the EEG series of channels F3 and F4 under the average reference montage. We then calculated PPSI on the frequency averaged inner product,

$$\mathrm{PPSI}_i = \frac{\sum_{k=t_s}^{t_e} y_i(k) I(y_i(k) > 0)}{\sum_{k=t_s}^{t_e} I(y_i(k) > 0)}, \text{where } y_i(k) = \frac{1}{20}\sum_{\lambda=5}^{24} y_{i,\lambda}(k).$$

We analyzed the distribution of the PPSI against all the IEDs labeled with and without preceding positive spike. The Kolmogorov-Smirnov test indicates a significant distribution difference between the two distributions. We chose the lower 5 % quantile of the PPSI distribution with positive discharge as the decision criteria.

2.7. Performance measures

The automatically detected IEDs were compared with the manual labels to evaluate their performance, where we treated the manual labels as the gold standard. We defined one detected IED correctly matched with the manual label when the time difference between their occurrences was within 0.1 s, and both occurrences were situated within the same hemisphere of Rolandic region. The basic unit of IED duration was defined to be 0.1 s. Sensitivity (SENS), specificity (SPEC), accuracy (ACC), precision (PREC) and F1-score were calculated following the conventional formula:

$$\mathrm{SENS} = \frac{\mathrm{TP}}{\mathrm{TP} + \mathrm{FN}},$$

$$\mathrm{SPEC} = \frac{\mathrm{TN}}{\mathrm{TN} + \mathrm{FP}},$$

$$\mathrm{ACC} = \frac{\mathrm{TP} + \mathrm{TN}}{\mathrm{TP} + \mathrm{TN} + \mathrm{FP} + \mathrm{FN}},$$

$$\mathrm{PREC} = \frac{\mathrm{TP}}{\mathrm{TP} + \mathrm{FP}},$$

$$\mathrm{F1} = \frac{2\mathrm{TP}}{2\mathrm{TP} + \mathrm{FP} + \mathrm{FN}},$$

where TP denotes the true positive for IEDs labeled by both epileptologists and the algorithm; TN for the true negative for normal period with no IEDs detected; FP the false positive for IEDs reported only by the algorithm; and FN for the false negative where IEDs reported by epileptologists but not by the algorithm. We note that since the clinical data were extremely imbalanced, the number of negative occasions were much larger than the positive occasions, which usually lead to a higher SPEC and ACC. In addition, we used the false alarm rate (FAR) to evaluate the performance in nonepileptic controls, which was the number of FP IEDs per hour.

3. Results

3.1. Cross-patient classification performance

In this subsection, we first evaluated the proposed IEDs detection procedure against the SeLECTS patients in the private test dataset. The proposed procedure detected 18,501 IEDs in the 19 h EEG records, where 17,758 of them were concordance with the labels provided by the epileptologists. The detailed patient level performance results reported in Table 2 indicated a good generalization ability. The average SENS, SPEC and ACC were 97.8 % (±2.7 %), 99.8 % (±0.1 %) and 99.8 % (±0.2 %), respectively. The standard deviation of SENS was relatively higher due to the outlier patient 07. Furthermore, when applied to the

Table 2
Sensitivity (SENS), specificity (SPEC), accuracy (ACC) and false alarm rate (FAR) per hour of the proposed method and three recently proposed algorithms.

Methods	SeLECTS patients				Nonepileptic controls		
	Patients	**SENS**	**SPEC**	**ACC**	**Patients**	**ACC**	**FAR**
The proposed method	01	99.0	99.7	99.6	09	100.0	0.0
	02	99.7	99.9	99.9	10	100.0	0.0
	03	98.6	99.7	99.5	11	100.0	1.5
	04	97.7	100.0	99.9	12	100.0	2.5
	05	98.4	100.0	100.0	13	100.0	5.5
	06	98.7	100.0	100.0	14	100.0	0.5
	07	91.4	99.8	99.7	15	100.0	0.8
	08	98.8	99.7	99.7	16	100.0	3.4
	average	97.8	**99.8**	**99.8**	average	**100.0**	**1.8**
Heers, et al. [33]		94.0	95.0	95.0			
Wu, et al. [26]		**98.2**	95.1	96.5			
Luo, et al. [17]		97.1	94.6	95.9			

22 h of nonepileptic EEG recordings in the test dataset, the proposed procedure detected 41 IEDs in total, corresponding to a FAR of 1.8 (±1.9) IEDs per hour. Since the 41 IEDs only affected 4.1 s EEG recordings, the corresponding ACC was 100.0 %. The dipole patterns have been detected in all the SeLECTS patients, whose occurrence frequency ranged from 73 % to 96 %.

To further validate the diurnal rhythm of IEDs, we quantified the discharge frequencies of the automatically detected IEDs during awake and sleep stages, as illustrated in Table 3. Due to the relatively short recording time (about 2–5 h), we did not capture sleep stage for patient 08. However, for the other SeLECTS patients who were monitored during both awake and sleep stages, a significant increasing in IEDs frequency was observed during sleep. The average IEDs frequency was 32 times higher during sleep as compared to the wakeful period, which was consistent with the prevailing understanding that discharges tend to intensify during sleep in SeLECTS [34].

3.2. Averaged waveform and the voltage map

By treating the whole procedure as a quantitative analysis tool, we can visualize the voltage maps, average waveform plots and dipole patterns from the detected IEDs. The average waveform was obtained by aligning the peak of each individual IEDs. Fig. 3 provides an illustrative example from a patient with unilateral Rolandic IEDs where the automated detection procedure mapped the IEDs to the right Rolandic area, predominantly at T4 > T6 > C4/P4, as evidenced in both bipolar and the average reference montages (Fig. 3A). The corresponding voltage map in Fig. 3B showed a dipole pattern of the central-temporal discharge, which was drawn according to the amplitude at the 0 s of the average reference montage. A negative voltage field appeared at the right central-temporal region (T4: −59.8 μV, C4: −13.6 μV), and the existence of a dipole pattern was confirmed by the positive field at the frontal region (Fp2: 28.1 μV). We used a 10 s segment to illustrate the detected IEDs in the raw EEG series (Fig. 2C). Finally, 7609 sharp waves were detected in around 4.7 h, corresponding to average frequency of 1605 discharges per hour.

Fig. 4 summarizes the procedure's performance in another SeLECTS patient with IEDs in bilateral Rolandic area. During the two hours recording, we detected 2204 IEDs in the left Rolandic area (Fig. 3A), and 2662 IEDs in the right (Fig. 4B). The absolute amplitudes of the IEDs were observed to be greater in the right Rolandic area (T4: −81.8 μV, C4: −54.8 μV) as compared to the left Rolandic area (P3: −65.3 μV, T5: −50.1 μV). Although the negative discharges were seen in the bilateral Rolandic area, the positive discharges usually occurred in the left frontal region, with the maximal positive voltage mapped at the F3 channel.

3.3. Cross-dataset evaluation

To extend the evaluation of the proposed procedure's performance to different types of epilepsy, we applied a cross-dataset evaluation, namely we trained the procedure on the private SeLECTS dataset while tested against the publicly available TUEV dataset (version 2.0.1). We formulate the procedure as a binary classification task by selecting SPSW, GPED and PLED as the IED classes, while the remaining classes EYEM, ARTF and BCKG were chosen as the negative classes. The TUEV dataset contained many IEDs occurred in the prefrontal channels Fp1 and Fp2. Thus, only EMG artifacts were removed, while all EOG signals were retained after the inverse ICA transform, different from the discussions in Section 2.3. As shown in Table 4, the proposed procedure maintained high detection specificity, matching the 99.8 % SPEC observed on the private dataset. However, due to the presence of a broader number of unseen IED types in the TUEV dataset, the SENS experienced a decline, falling from 97.8 % to 85.4 %. Despite this reduction, due to the maintained high specificity, both the ACC and the F1 score remained high, thereby demonstrating the robustness of the model in the cross-dataset evaluation.

4. Discussion

By applying the transformer architecture, clinical knowledge-based waveform dictionary and the automatic artifact removal technique offered by the ICA, we have developed an efficient deep learning procedure to identify the temporal occurrence and the specific EEG electrodes activated by each individual IED embedded in the raw EEG

Table 3
Descriptive statistics of the IEDs during sleep and awake periods. The IEDs frequency was a standardized IED numbers per hour.

Patients	Sleep duration	IEDs number	frequency	Awake duration	IEDs number	frequency
01	1:35:46	3554	2227	0:02:12	0	0
02	0:39:27	3562	5417	1:20:34	93	69
03	0:52:13	5192	5966	1:07:47	89	79
04	0:02:40	31	698	1:57:20	1003	513
05	0:55:48	1152	1239	4:26:01	221	50
06	1:06:34	1874	1689	1:13:17	194	159
07	0:46:02	345	450	1:13:58	453	367
08	–	–	–	2:00:00	267	134

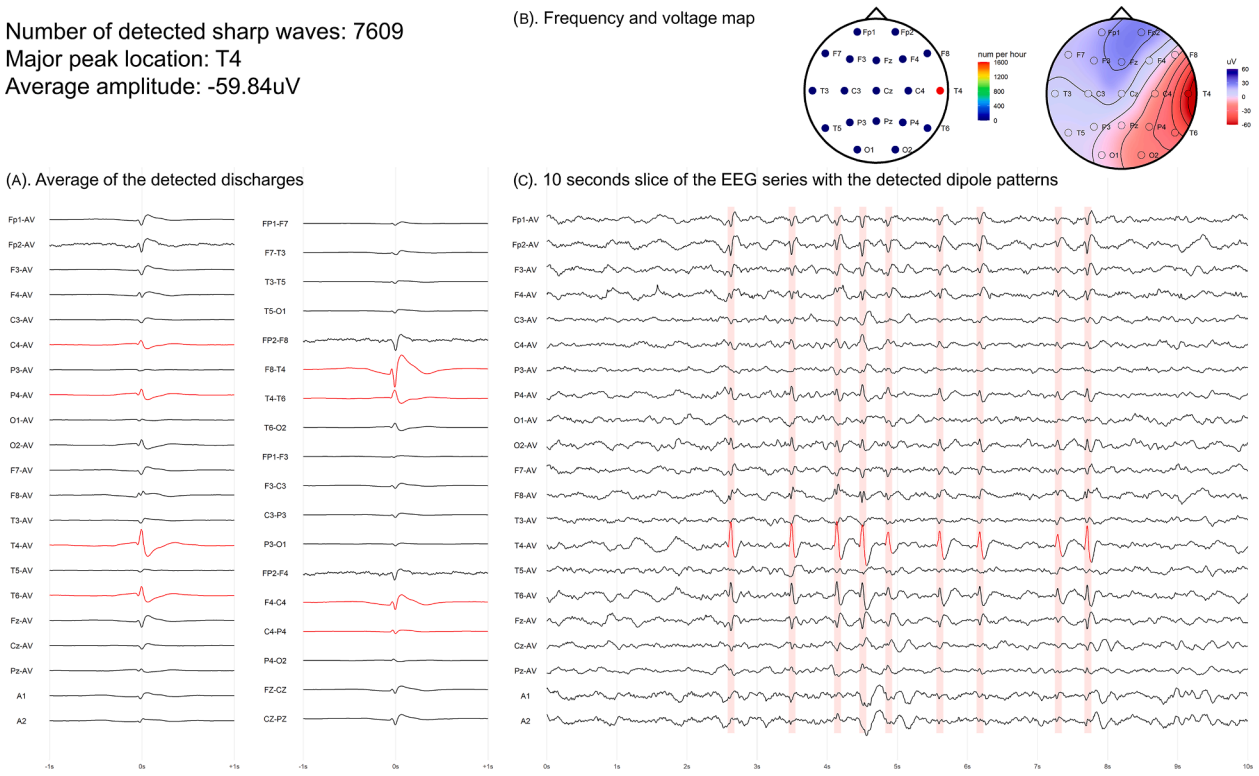

Fig. 3. The detected sharp wave with dipole patterns in patient with unilateral Rolandic IEDs. (A) the averaged waveform in the averaged referential montage and the bipolar montage. (B) The discharge frequency and the voltage map. The voltage map was calculated by the averaged referential montage at the 0 s of the subplot (A). (C) A 10 s slice of the raw EEG series, where the detected sharp waves were marked as red.

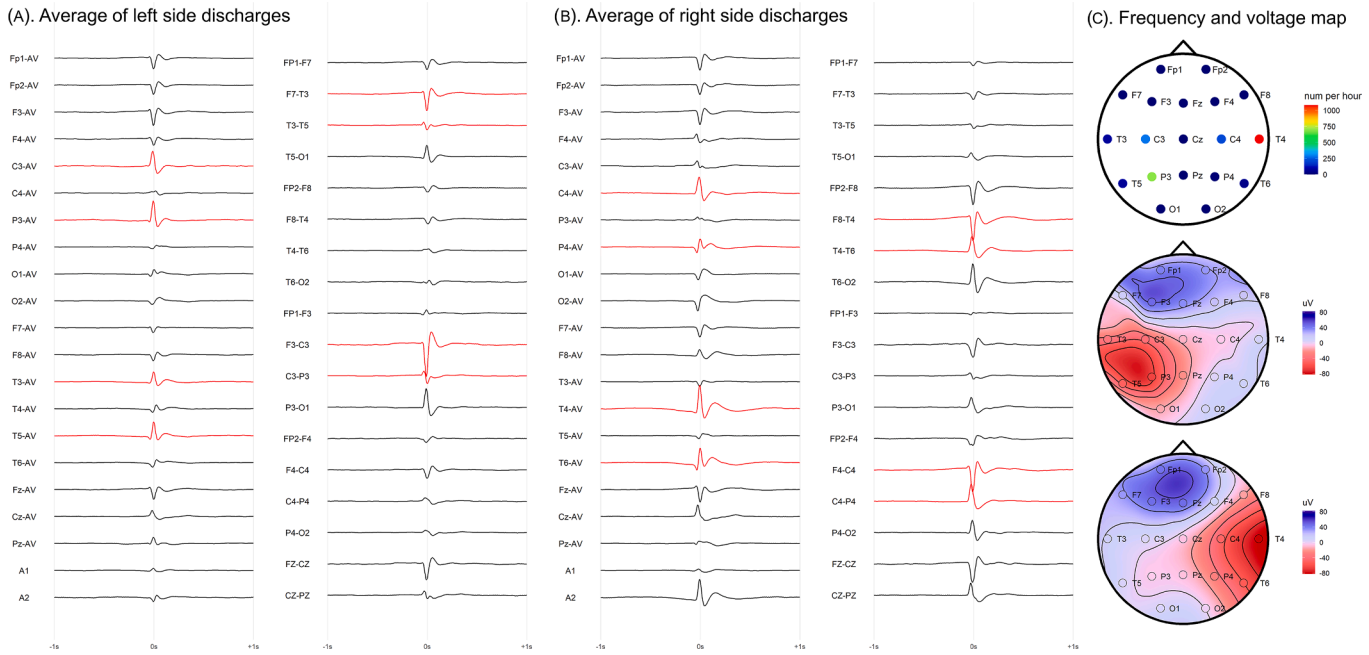

Fig. 4. The detected sharp wave with dipole patterns in patient with IEDs in bilateral Rolandic areas. (A) the averaged waveform in the averaged referential montage and the bipolar montage at the left hemisphere. (B) The same as (A) but in the right hemisphere. (C) The discharge frequency and the voltage map. The voltage map was calculated by the averaged referential montage at the 0 s of the subplots (A) and (B).

recordings, which could be used in counting and comparing IEDs in future study of epilepsy.

The proposed procedure achieved good performance with a sensitivity of 97.8 % and a specificity of 99.8 % in the cross-patient evaluation. It is known that the machine learning methods may suffer from overfitting and the model performance may decrease on the test data due to the existence of covariant shift. However, since we spilt the test and training dataset at the patient level, our procedure has fully considered the effect of inter-individual variability, which further enhanced the model's practicality. We also compared the proposed

Table 4
Sensitivity (SENS), specificity (SPEC), accuracy (ACC), precision (PREC) and F1 score of the proposed method and five recently proposed algorithms.

Methods	SENS	SPEC	ACC	PREC	F1	validation type
The proposed procedure	85.4	**99.8**	**95.8**	**99.4**	**91.9**	cross-dataset
Nhu, et al. [23]	65.0			88.0	75.0	cross-dataset
Wang, et al. [35]					88.0	within-dataset
Golmohammadi, et al. [36]	90.1	95.1				within-dataset
Munia, et al. [37]	85.9			88.5	87.2	within-dataset
Sabor, et al. [38]	**95.4**	95.5	95.5	87.3	91.2	within-dataset

method with the accuracy reported by other IEDs detection algorithms (Table 2). Heers, et al. [33] evaluated on the original proportion of data segments without resampling the imbalanced labels. Their automatically detected IED types contained several physiological transients, which still required subsequent manual review. Wu, et al. [26] and Luo, et al. [17] resampled the data segments to achieve a balance between epileptic and normal samples, which was helpful for SENS, but their SPEC and ACC were still not high enough. In comparison, the proposed procedure utilized the transformer architecture and the multi-head attention mechanism in building the deep learning classifier. Compared with other widely used classifiers, transformer can capture the time dependence, automatically assigns weight to the important period. Furthermore, the multiple attention heads allow the procedure attending different parts of the EEG series, like the spike part and the following slow wave. The transformer, combined with the knowledge-based waveform features, achieved attractive generalization ability.

Moreover, using the proposed automatic IEDs detection procedure, we have the ability to fast quantify the number of IEDs during the sleep-waking cycle. It is known that SeLECTS is characterized by an increase in IED frequency during sleep compared with the awake stage [34]. The statistical analysis of IEDs in different periods is of great importance in the study of epilepsy and is made possible by the proposed automated detection. It has been reported that the frequency of discharges is a measure of the severity of epileptiform activity [39]. Our algorithm provided a robust mean of IED quantification, which might help in the future study of epilepsy treatment.

As demonstrated in the cross-dataset evaluation, the proposed procedure could be extended to other types of epilepsy. Compared with the existing methods, the proposed procedure achieved the best SPEC, ACC, PREC and F1-score, with the SENS ranked fourth in the TUEV dataset. The occurrence location and waveform of IEDs may vary across different epilepsy types, resulting in reduced SENS in the context of previously unseen IED types. Nonetheless, due to the similarity in the artifacts, eye movements, and background neural activities captured during the monitoring of the normal brain function without epileptiform occurrences, the procedure maintained robust specificity. This robustness was achieved by training with the 26 normal EEG recordings featured with nonepileptiform sharp transients. We note that the proposed procedure detected IEDs separately in each of the 19 EEG channels. The IEDs were mapped to the channel with the maximum discharge amplitude in each of the brain region. Although one can further improve SPEC by simply excluding the IEDs beyond the Rolandic region for SeLECTS patients, the cross-dataset testing performance suggested that the proposed procedure may have a stronger adaptability to other types of epilepsy.

Furthermore, although SeLECTS exhibits high amplitude, its discharge morphology is similar from typical IEDs in focal epilepsy, with only some different etiology and statistical differences noted [40]. The proposed algorithm shows outstanding advantages in identifying positive discharges specific as a biomarker in SeLECTS diagnostics, but requires further validation in other conditions. The dipole patterns may appear in SeLECTS, Panayiotopoulos Syndrome (PS), and other types of epilepsy, which are of great importance in the understanding of the discharge propagation [41–43]. In our study, precise localization of the dipole patterns has been achieved using the average waveform plot. The EEG dipole source localization not only help with the diagnosis of SeLECTS and PS, but provides a tool for improved non-invasive localization of epileptogenic foci [44]. Thus, our algorithm in detection of dipole is practical for prolonged VEEG recordings which are typically acquired for clinical purposes.

5. Conclusion

This study proposes a fully automated IEDs detection algorithm which achieves both high accuracy and high temporal resolution. Quantitative statistics such as the IEDs frequency, voltage map, circadian rhythms and averaged morphological features can be readily extracted from the detection outputs of the procedure. These detailed statistics open opportunities for future clinical research to refine predictive methods, such as enhancing the predictive efficacy of antiseizure medication responses by substituting binary EEG abnormality indicators with precise measures of IED frequency.

Our study also had limitations. Firstly, the study is based on a relatively small sample size. Secondly, EEG acquisition systems were from the same company in two centers, and additional study sites with other EEG acquisition systems should be included in the future. Thirdly, the scalp-visible IEDs represent about 45 % (in high-density EEG) to 20 % (in 19 channel 10–20 system) of intracranial IEDs elicited in the brain due to the low skull conductivity [12], such IEDs might be more effectively captured using intracranial EEG. Future works can be made to remove these limitations. EEG source localization techniques could also be used to reconstruct the intracranial IEDs signals, thereby transcending mere scalp EEG electrode mapping to locate their precise cerebral origins.

Funding statement

This research was supported by the National Natural Science Foundation of China (12026607 and 12071013).

7. Ethics Statement

We confirm that we have read the Journal's position on issues involved in ethical publication and affirm that this report is consistent with those guidelines.

8. Ethics approval statement

This study involves human participants complied with the declaration of Helsinki and has gained approval by the Ethics Committee of West China Hospital of Sichuan University (2022169) and the Ethics Committee of Chengdu Women's and Children's Central Hospital (2023109).

9. Patient consent statement

Informed consent was exempted by the boards.

10. Clinical trial registration

This study is registered at the Chinese Clinical Trial Register under the title "Neural mechanism modeling and data assisted diagnosis and treatment algorithms for children with brain development disorders" (ChiCTR2200065513) on January 29th, 2022, https://www.chictr.org.cn/bin/project/edit?pid=175587.

CRediT authorship contribution statement

Peifeng Tong: Writing – original draft, Software, Methodology, Formal analysis, Data curation, Conceptualization. **Bosi Dong:** Writing – review & editing, Validation, Investigation, Data curation, Conceptualization. **Xiangdong Zeng:** Data curation, Conceptualization. **Lei Chen:** Supervision, Resources, Project administration, Funding acquisition, Conceptualization. **Song Xi Chen:** Writing – review & editing, Supervision, Resources, Project administration, Funding acquisition, Conceptualization.

Declaration of competing interest

The authors declare that they have no known competing financial interests or personal relationships that could have appeared to influence the work reported in this paper.

Acknowledgement

This research was supported by the National Natural Science Foundation of China (12026607 and 12071013). We would also like to thank Luyan Huang and Qiulei Hong from West China Hospital for their valuable collaboration in data acquisition.

Appendix A. Supplementary data

Supplementary data to this article can be found online at https://doi.org/10.1016/j.bspc.2024.107238.

Data availability

The datasets used and/or analyzed during the current study are available from the corresponding authors on reasonable request (Song Xi Chen, E-mail: csx@gsm.pku.edu.cn and Lei Chen, E-mail: leilei_25@126.com).

References

[1] R.L. Casali, et al., Comparison of auditory event-related potentials between children with benign childhood epilepsy with centrotemporal spikes and children with temporal lobe epilepsy, Epilepsy & Behavior 59 (2016) 111–116.
[2] X.-Y. Shi, et al., Identification of susceptibility variants to benign childhood epilepsy with centro-temporal spikes (BECTS) in Chinese Han population, EBioMedicine 57 (2020) 102840.
[3] L.C. Mellish, C. Dunkley, C.D. Ferrie, D.K. Pal, Antiepileptic drug treatment of rolandic epilepsy and Panayiotopoulos syndrome: clinical practice survey and clinical trial feasibility, Archives of Disease in Childhood 100 (1) (2015) 62–67.
[4] B. Dalla Bernardina, et al., Sleep and benign partial epilepsies of childhood: EEG and evoked potentials study, Epilepsy Research. Supplement 2 (1991) 83–96.
[5] E.C. Wirrell, Benign epilepsy of childhood with centrotemporal spikes, Epilepsia 39 (s4) (1998) S32–S41, https://doi.org/10.1111/j.1528-1157.1998.tb05123.x.
[6] N. Specchio, et al., International League Against Epilepsy classification and definition of epilepsy syndromes with onset in childhood: Position paper by the ILAE Task Force on Nosology and Definitions, Epilepsia 63 (6) (2022) 1398–1442.
[7] M. Janmohamed *et al.*, "Moving the field forward: detection of epileptiform abnormalities on scalp electroencephalography using deep learning—clinical application perspectives," *Brain Communications,* vol. 4, no. 5, 2022, doi: 10.1093/braincomms/fcac218.
[8] J. Thomas, et al., Automated Detection of Interictal Epileptiform Discharges from Scalp Electroencephalograms by Convolutional Neural Networks, International Journal of Neural Systems 30 (11) (2020) 2050030, https://doi.org/10.1142/s0129065720500306.
[9] M. Abou Jaoude, et al., Detection of mesial temporal lobe epileptiform discharges on intracranial electrodes using deep learning, Clinical Neurophysiology 131 (1) (2020) 133–141, https://doi.org/10.1016/j.clinph.2019.09.031.
[10] C. da Silva Lourenço, M.C. Tjepkema-Cloostermans, M.J.A.M. van Putten, "Machine learning for detection of interictal epileptiform discharges,", Clinical Neurophysiology 132 (7) (2021) 1433–1443, https://doi.org/10.1016/j.clinph.2021.02.403.
[11] E.E.M. Reus, F.M.E. Cox, J.G. van Dijk, G.H. Visser, Automated spike detection: Which software package? Seizure 95 (2022) 33–37, https://doi.org/10.1016/j.seizure.2021.12.012.
[12] B. Abdi-Sargezeh, et al., A review of signal processing and machine learning techniques for interictal epileptiform discharge detection, Computers in Biology and Medicine 168 (2024) 107782, https://doi.org/10.1016/j.compbiomed.2023.107782.
[13] J.R. Stevens, B.L. Lonsbury, S.L. Goel, Seizure Occurrence and Interspike Interval: Telemetered Electroencephalogram Studies, Archives of Neurology 26 (5) (1972) 409–419, https://doi.org/10.1001/archneur.1972.00490110043004.
[14] J. Thomas, J. Jin, J. Dauwels, S. S. Cash, and M. B. Westover, "Automated epileptiform spike detection via affinity propagation-based template matching," in *2017 39th Annual International Conference of the IEEE Engineering in Medicine and Biology Society (EMBC)*, 11-15 July 2017 2017, pp. 3057-3060, doi: 10.1109/EMBC.2017.8037502.
[15] M.A. Kural, et al., Accurate identification of EEG recordings with interictal epileptiform discharges using a hybrid approach: Artificial intelligence supervised by human experts, Epilepsia 63 (5) (2022–05-01 2022,) 1064–1073, https://doi.org/10.1111/epi.17206.
[16] C. Cheng, et al., Multilevel Feature Learning Method for Accurate Interictal Epileptiform Spike Detection, IEEE Transactions on Neural Systems and Rehabilitation Engineering 30 (2022) 2506–2516, https://doi.org/10.1109/TNSRE.2022.3193666.
[17] T. Luo, et al., EMD-WOG-2DCNN based EEG signal processing for Rolandic seizure classification, Computer Methods in Biomechanics and Biomedical Engineering 25 (14) (2022–10-26 2022,) 1565–1575, https://doi.org/10.1080/10255842.2021.2023809.
[18] R.J. Quon, et al., AiED: Artificial intelligence for the detection of intracranial interictal epileptiform discharges, Clinical Neurophysiology 133 (2022) 1–8, https://doi.org/10.1016/j.clinph.2021.09.018.
[19] M. McDougall, H. Albaqami, G. M. Hassan, and A. Datta, "Patient Independent Interictal Epileptiform Discharge Detection," in *2023 45th Annual International Conference of the IEEE Engineering in Medicine & Biology Society (EMBC)*, 24-27 July 2023 2023, pp. 1-6, doi: 10.1109/EMBC40787.2023.10341194.
[20] A.H. Mohammed, M. Cabrerizo, A. Pinzon, I. Yaylali, P. Jayakar, M. Adjouadi, Graph neural networks in EEG spike detection, Artificial Intelligence in Medicine 145 (2023) 102663, https://doi.org/10.1016/j.artmed.2023.102663.
[21] K. Fukumori, N. Yoshida, H. Sugano, M. Nakajima, T. Tanaka, Satelight: self-attention-based model for epileptic spike detection from multi-electrode EEG, Journal of Neural Engineering 19 (5) (2022/09/23 2022,) 055007, https://doi.org/10.1088/1741-2552/ac9050.
[22] Y. Roy, H. Banville, I. Albuquerque, A. Gramfort, T.H. Falk, J. Faubert, Deep learning-based electroencephalography analysis: a systematic review, Journal of Neural Engineering 16 (5) (2019/08/14 2019,) 051001, https://doi.org/10.1088/1741-2552/ab260c.
[23] D. Nhu, et al., Automated Interictal Epileptiform Discharge Detection from Scalp EEG Using Scalable Time-series Classification Approaches, International Journal of Neural Systems 33 (01) (2023) 2350001, https://doi.org/10.1142/s0129065723500016.
[24] B. Wei, X. Zhao, L. Shi, L. Xu, T. Liu, J. Zhang, A deep learning framework with multi-perspective fusion for interictal epileptiform discharges detection in scalp electroencephalogram, Journal of Neural Engineering 18 (4) (2021/07/21 2021,) pp. 0460b3, https://doi.org/10.1088/1741-2552/ac0d60.
[25] S.N. Chandrasekaran, H. Ceulemans, J.D. Boyd, A.E. Carpenter, Image-based profiling for drug discovery: due for a machine-learning upgrade? Nature Reviews Drug Discovery 20 (2) (2021/02/01 2021,) 145–159, https://doi.org/10.1038/s41573-020-00117-w.
[26] D. Wu *et al.*, "BECT Spike Detection Algorithm Based on Optimal Template Matching and Morphological Feature Selection," *IEEE Transactions on Circuits and Systems II: Express Briefs,* vol. 69, no. 4, pp. 2366-2370, 2022-04-01 2022, doi: 10.1109/tcsii.2022.3151486.
[27] P.F. Tong, H.X. Zhan, S.X. Chen, Ensembled Seizure Detection Based on Small Training Samples, IEEE Transactions on Signal Processing 72 (2024) 1–14, https://doi.org/10.1109/TSP.2023.3333546.
[28] A. Vaswani, et al., Attention is all you need, Advances in Neural Information Processing Systems 30 (2017).
[29] A. Harati, M. Golmohammadi, S. Lopez, I. Obeid, and J. Picone, "Improved EEG event classification using differential energy," in *2015 IEEE Signal Processing in Medicine and Biology Symposium (SPMB)*, 12-12 Dec. 2015 2015, pp. 1-4, doi: 10.1109/SPMB.2015.7405421.
[30] A. Hyvarinen, Fast and robust fixed-point algorithms for independent component analysis, IEEE Transactions on Neural Networks 10 (3) (1999–05-01 1999,) 626–634, https://doi.org/10.1109/72.761722.
[31] G.P. Nason, Wavelet Methods in Statistics with R, Springer Publishing Company, Incorporated, 2008.
[32] F.A. Nascimento, J.D. Barfuss, A. Jaffe, M. Brandon Westover, J. Jing, A quantitative approach to evaluating interictal epileptiform discharges based on interpretable quantitative criteria, Clinical Neurophysiology 146 (2023) 10–17, https://doi.org/10.1016/j.clinph.2022.10.018.
[33] M. Heers, et al., Detection of interictal epileptiform discharges in an extended scalp EEG array and high-density EEG—A prospective multicenter study, Epilepsia 63 (7) (2022–07-01 2022,) 1619–1629, https://doi.org/10.1111/epi.17246.
[34] B. Jin, T. Aung, Y. Geng, S. Wang, Epilepsy and Its Interaction With Sleep and Circadian Rhythm, (in English), *Frontiers in Neurology,* Review 11 (2020), https://doi.org/10.3389/fneur.2020.00327.
[35] Q. Wang, S. Whitmarsh, V. Navarro, T. Palpanas, iEDeaL: A Deep Learning Framework for Detecting Highly Imbalanced Interictal Epileptiform Discharges, Proc. VLDB Endow. 16 (3) (2022) 480–490, https://doi.org/10.14778/3570690.3570698.
[36] M. Golmohammadi, A.H. Harati Nejad Torbati, S. Lopez de Diego, I. Obeid, J. Picone, Automatic Analysis of EEGs Using Big Data and Hybrid Deep Learning

Architectures (in English), *Frontiers in Human Neuroscience,* Technology Report 13 (2019), https://doi.org/10.3389/fnhum.2019.00076.

[37] M. S. Munia, M. Nourani, J. Harvey, and H. Dave, "Interictal Epileptiform Discharge Detection Using Multi-Head Deep Convolutional Neural Network," in *2023 45th Annual International Conference of the IEEE Engineering in Medicine & Biology Society (EMBC)*, 24-27 July 2023 2023, pp. 1-4, doi: 10.1109/EMBC40787.2023.10340735.

[38] N. Sabor, Y. Li, Z. Zhang, Y. Pu, G. Wang, Y. Lian, Detection of the interictal epileptic discharges based on wavelet bispectrum interaction and recurrent neural network, Science China Information Sciences 64 (6) (2021/04/27 2021,) 162403, https://doi.org/10.1007/s11432-020-3100-8.

[39] M. Urbanska, et al., GSK3β activity alleviates epileptogenesis and limits GluA1 phosphorylation, eBioMedicine 39 (2019) 377–387, https://doi.org/10.1016/j.ebiom.2018.11.040.

[40] A. V. Misiukas Misiūnas, T. Meškauskas, and R. Samaitienė, "Algorithm for automatic EEG classification according to the epilepsy type: Benign focal childhood epilepsy and structural focal epilepsy," *Biomedical Signal Processing and Control,* vol. 48, pp. 118-127, 2019-02-01 2019, doi: 10.1016/j.bspc.2018.10.006.

[41] H. Yoshinaga, K. Kobayashi, T. Akiyama, T. Shibata, F. Endoh, Y. Ohtsuka, Clinical implications of preceding positive spikes in patients with benign partial epilepsy and febrile seizures, Brain and Development 35 (4) (2013) 299–306, https://doi.org/10.1016/j.braindev.2012.06.006.

[42] H. Yoshinaga *et al.*, "EEG Dipole Characteristics in Panayiotopoulos Syndrome," *Epilepsia,* vol. 47, no. 4, pp. 781-787, 2006-04-01 2006, doi: 10.1111/j.1528-1167.2006.00519.x.

[43] H. Daou, F. Labeau, EEG Compression of Scalp Recordings Based on Dipole Fitting, IEEE Journal of Biomedical and Health Informatics 19 (3) (2015) 995–1008, https://doi.org/10.1109/JBHI.2014.2346493.

[44] S. Meckes-Ferber, A. Roten, C. Kilpatrick, T.J. O'Brien, EEG dipole source localisation of interictal spikes acquired during routine clinical video-EEG monitoring, Clinical Neurophysiology 115 (12) (2004) 2738–2743, https://doi.org/10.1016/j.clinph.2004.06.023.